



Application of enzyme-mediated cellulose nanofibers from lemongrass waste for the controlled release of anticancer drugs

Priyanka Kumari^{1,2} · Abha Meena^{1,2}

Received: 20 November 2019 / Accepted: 6 March 2020 / Published online: 25 March 2020
© Springer-Verlag GmbH Germany, part of Springer Nature 2020

Abstract

In the present study, an application of cellulose nanofibers has been established for the controlled release of an anticancer drug, i.e., camptothecin. The camptothecin is known for its antitumor activity. However, it has certain limitations like instability, low solubility in aqueous solution, and biological fluids. Firstly, the camptothecin was encapsulated into the cellulose nanofiber complex by adjusting the composition ratio of cellulose nanofibers—camptothecin, i.e., 10:3, 10:5, and 10:7. In the 10:3 composition ratio of cellulose nanofibers, camptothecin showed the highest encapsulation efficiency, i.e., 65.28%. The binding of camptothecin with cellulose nanofibers was confirmed by FT-IR analysis. Also, the Langmuir, Freundlich, Temkin, and Dubinin-Radushkevich isotherm studies demonstrate physical adsorption of camptothecin onto the homogeneous as well as the heterogeneous surface of cellulose nanofibers. Further, the controlled and extended-release profile was observed at different physiological pH, and different kinetics models were used to understand the drug release mechanism. The highest correlation in all pH conditions was obtained in Korsmeyer-Peppas with R^2 value = 0.93 (pH 1.2), 0.89 (pH 6.8), and 0.97 (pH 7.4), whereas in Higuchi model, R^2 value = 0.89 (pH 1.2), 0.91 (pH 6.8), and 0.98 (pH 7.4), suggesting the release of a drug via a diffusion mechanism. Hence, the results established that enzyme-mediated cellulose nanofibers may also be an optimal carrier for the controlled drug release formulation without any chemical excipients.

Keywords Cellulose · Nanocarrier · Camptothecin · Controlled release · Isotherm · Kinetic

Introduction

The cellulose is an abundantly available natural polymer. The cellulose nanofibers (CNF) are generally isolated from various agricultural biomass and renewable waste (Cherian et al. 2008; Deepa et al. 2015). Usually, the waste is hardly utilized and mostly burned, which lead to a massive release of pollutants in the air and deteriorate the soil fertility. An alternative approach for efficient utilization is in the paper and pulp, textile industries, or as animal feed (Salah 2013; Bardet and Bras 2014). The lemongrass waste after oil extraction is of limited use, such as

animal feed and composting, which is not a cost-effective approach. Every year, almost 30,000,000 tons of residual biomass produced at the farmer's field (Kaur et al. 2010). The green synthesis of nanofibers using agricultural waste could be an eco-friendly and cost-effective approach to utilize tons of agricultural waste. Therefore, enzyme-mediated nanofiber synthesis has gained immense importance, as it is a milder treatment and does not require prolonged steps and chemicals (Filson et al. 2009; Kumari et al. 2019).

Nanoparticle-based drug delivery has gained importance, especially sustained and targeted release systems are undergoing rapid development by employing various experimental approaches (Costache et al. 2009). The production of nanofibers is one of the unique findings in the field of nanotechnology. Natural polymers have gained more interest in controlled drug delivery compared with synthetic polymers due to biodegradability, biocompatibility, availability, and low toxic properties (Esmaeili and Rafiee 2015; Clift et al. 2011; Pereira et al. 2013). Compared with traditional medicinal formulations, the fiber-based drug carrier system has numerous advantages like effective drug therapy and controlled release

Responsible Editor: Tito Roberto Cadaval Jr

✉ Abha Meena
a.meena@cimap.res.in

¹ Molecular Bioprospection Department, CSIR-Central Institute of Medicinal and Aromatic Plants, Lucknow, Uttar Pradesh 226015, India

² Academy of Scientific & Innovative Research (AcSIR), Ghaziabad 201002, India

of drugs with reduced toxicity (Zeng et al. 2003; Hu et al. 2014). Nanofibers are extensively used in biomedicine as a carrier system for controlled drug delivery due to unique properties like large surface area, high porosity, flexibility, and economic (Kentaro Abe et al. 2007). The high surface to volume ratio of the nanofibers helps in improving the encapsulation and transportation of drugs (Mehrabi et al. 2017).

The application of CNF as a drug carrier is in high demand, therefore needing to be explored. Controlled drug delivery systems have been used to overcome the challenges of conventional drug formulations. The controlled drug delivery systems allow the delivery of drugs at fixed rates for a predefined time interval (Ali and Ahmed 2018). The nanofibers are utilized in various areas like dental applications, wound healing, drug delivery, and tissue engineering (Bhandari et al. 2017). Besides, due to the presence of multiple binding sites, nanofibers serve as a carrier system for the different drugs like antioxidants, antimicrobials, flavors, enzymes, and functional group compounds (Fonseca et al. 2019; Li et al. 2019; Rezaei et al. 2015; Löbmann and Svagan 2017). These nanofibers protect, stabilize, and prevent aggregation of the compounds, which proves to be beneficial in the controlled release (Bhandari et al. 2017; Valo et al. 2011). The poor solubility of drugs is a known challenge during the drug formulation for drug delivery systems. The camptothecin (CPT) is a plant-based alkaloid, which is available naturally in the stem and bark of *Camptotheca acuminata*. It has shown antitumor activities against several tumor types (Çirpanli et al. 2009). However, the poor solubility (Gao et al. 2008), instability of lactone ring, toxicity (Natesan et al. 2014), non-tumorigenic actions, rapid clearance (Mi and Burke 1994), and stability at different physiological conditions (Fan et al. 2010) hinder its medical usage. Hence, the need for novel excipients to overcome challenges in drug formulations is continuous (Löbmann and Svagan 2017).

The effectiveness of nanostructures as a drug carrier system is generally affected by the shape, size, and other biophysical/chemical characteristics. For example, polymeric nanomaterials with diameters ranging between 10 and 1000 nm, displayed properties, ideal for an effective carrier system (Silva et al. 2013). In various studies, the CNF has been utilized for the formulation of poorly soluble drugs and considered a promising excipient (Löbmann and Svagan 2017). As a natural nanocarrier, the CNF shows promising potentials in enhancing the efficacy of the drug (Lin and Dufresne 2014). The use of an enzyme-hydrolyzed CNF as a carrier system to effectively encapsulate camptothecin and release the drug in controlled and extended patterns has not been explored previously. Considering the properties of CNF, the aim of the present study is to explore the potential of enzyme-mediated synthesized CNF as a drug nanocarrier. To explore the hypothesis, CPT was taken as an example drug, and its encapsulation efficiency was measured at different

composition ratios. FT-IR and isotherm models were employed to explore the drug binding and its mechanism. Further, the controlled release characteristics without the appearance of burst effects and drug release mechanisms were explored using drug release kinetics models.

Materials and methods

Materials

Lemongrass biomass after oil extraction was used as a raw material for the production of cellulose, and later, it was used for the production of CNF. The CNF was prepared according to the protocol published by our group previously (Kumari et al. 2019). The lignocellulosic biomass of lemongrass waste was washed, oven-dried (60 °C) until completely dried, and chopped. Further, the material was exposed to the steam explosion along with 2% NaOH in an autoclave. Then, the material was washed with distilled water until neutral pH followed by de-lignification with 1% acidified sodium chlorite solution at 70 °C for 3 h. The obtained material was washed with distilled water until neutral pH and oven-dried. Then, the resultant fibers were subjected to enzymatic hydrolysis to obtain the CNF. The resultant material was dispersed in 50 mM sodium citrate buffer at pH 4.8, followed by stirring. The enzyme was added to the suspension of cellulose and stirred at 50 °C for 24 h. The reaction was stopped by boiling the sample for 10 min followed by centrifugation and rinsed with a buffer solution of pH 7.4. Then, the material was washed with deionized water and sonicated. The final product was freeze-dried and used for further experiments.

Chemicals

The solvent DMSO was purchased from Merck. The camptothecin was purchased from Sigma-Aldrich. All reagents were of analytical grade or higher.

Preparation of CNF-CPT formulations

The enzyme-hydrolyzed CNF, which was synthesized from biomass of lemongrass, was used in the experiment (Kumari et al. 2019). First, the CNF was dispersed in deionized water, followed by continuous stirring until the complete suspension. The CPT was loaded onto CNF according to the method previously described with few modifications (Nguyen et al. 2015). The diagrammatic representation of the preparation of formulations using CNF has been shown in Fig. 1. The different amounts of CPT, i.e., 3 mg, 5 mg, and 7 mg, were dissolved in DMSO and mixed with 10 mg of CNF dropwise and continuously stirred at room temperature for the binding of CPT and CNF. Then, the samples were centrifuged for

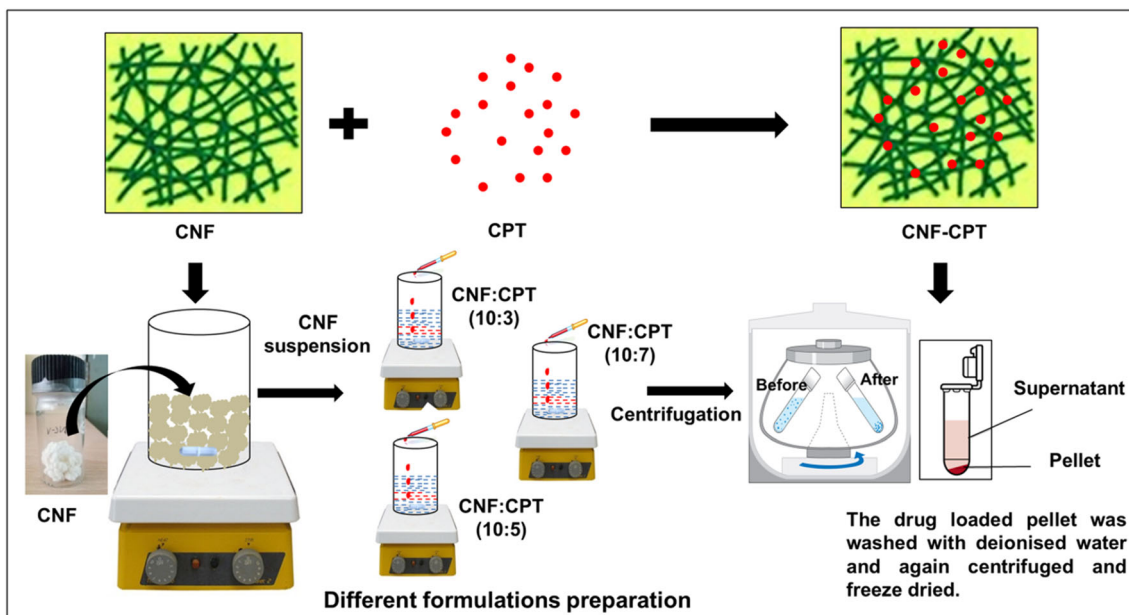


Fig. 1 Diagrammatic representation of the preparation of formulations. Cellulose nanofibers (CNF), camptothecin (CPT), and cellulose nanofibers and camptothecin composite (CNF-CPT)

15 min at 10,000 rpm and 4 °C, followed by washing with deionized water. The resultant material was freeze-dried and stored at 4 °C in the closed glass vial. The lyophilized CPT-loaded CNF was re-dispersed in distilled water as per the experimental requirements.

Characterization

The surface morphology of all the samples was studied by SEM (QUANTA 250, FEI). The interaction between the drug and CNF was estimated by the Fourier transform-infrared spectroscopy (FT-IR) instrument (PerkinElmer Spectrum BX). The particle size and polydispersity index of the prepared drug-loaded formulations was determined by dynamic light scattering (DLS) technique (Mastersizer 2000, Malvern Instruments, UK).

In vitro quantification of camptothecin

The stock solution of 1 mg/ml of CPT in DMSO was prepared. The stock solution of CPT was serially diluted to obtain five different working concentrations, i.e., 100, 10, 1, 0.1, and 0.01 µg/ml of CPT, to establish a calibration curve. The absorbance was measured at 367 nm using a UV spectrophotometer (Epoch 2 Microplate Spectrophotometer, BioTek Instruments). The regression equation was expressed as $y = 0.0084x + 0.0168$, $R^2 = 0.999$ (Fig. 3a). Each experiment was performed in triplicate.

Encapsulation efficiency and drug loading capacity of camptothecin

The CPT was used as a model drug for drug loading and release studies. The freeze-dried samples of different composition ratio CPT-CNF formulation were dispersed in dimethyl sulfoxide (DMSO) solvent. The samples were continuously stirred for 2 h and sonicated for 1 h for complete drug dissolution. The samples were centrifuged, and drug content in the supernatant was determined spectrophotometrically at 367 nm using a UV-visible spectrophotometer. The pellet was again re-dispersed in the solvent, followed by a similar method, and drug content was determined. The loading efficiency was calculated with respect to the final amount of drug entrapped in the CNF to the initial quantity of drug used during encapsulation experiments (Eq. 1). The loading capacity was calculated with respect to the final amount of drug entrapped in the CNF to the weight of the nanoparticles (Eq. 2).

Loading efficiency(%) (1)

$$= \frac{\text{Total amount of drug entrapped in pellet}}{\text{initial amount of drug taken for drug loading}} \times 100$$

Loading capacity (%) = $\frac{\text{Entrapped drug}}{\text{weight of the nanoparticles}} \times 100$ (2)

Adsorption isotherm studies

The equilibrium isotherm could be applied to determine the adsorption mechanism between the drug and carrier systems (Huang and Chen 2009). The two-parameter equations like Langmuir, Freundlich, Temkin, and Dubinin-Radushkevich were applied to analyze the equilibrium isotherm data. The assumption of Langmuir isotherm is homogeneous monolayer coverage of the adsorbate on to the adsorbent, similar energy of adsorption for all sites, free from any binding energy, and no interaction among the adsorbate molecules (Vázquez et al. 2007). The linearized equation of Langmuir isotherm was expressed as Eq. 3.

$$\frac{1}{Q_e} = \frac{1}{Q_0} + \frac{1}{Q_0 \cdot b \cdot C_e} \quad (3)$$

$$R_L = \frac{1}{1 + (1 + b \cdot C_0)} \quad (4)$$

where Q_e is the amount of adsorbate adsorbed per gram of the sorbent at equilibrium, Q_0 is the maximum monolayer adsorption (mg/g adsorbent), b is the Langmuir equilibrium constant (L/g adsorbent), C_0 is the initial concentration of adsorbate, and R_L is the separation factor.

The Freundlich isotherm describes the multilayer heterogeneous coverage onto the surface of the adsorbent with different adsorption sites (Vasudevan and Lakshmi 2012; Vasudevan et al. 2013). The isotherm predicts the adsorption intensity based on the $1/n$ value, i.e., $n = 1$ indicates heterogeneous surface, $1/n < 1$ indicates normal adsorption, and $1/n > 1$ indicates cooperative adsorption (Shaker and Yakout 2016). The linearized form of Freundlich model is expressed in Eq. 5.

$$\log Q_e = \log K_f + \frac{1}{n} \log C_e \quad (5)$$

where K_f is the Freundlich constant ($\text{mg g}^{-1}(\text{mg L}^{-1})^{-1/n}$) and $1/n$ is the heterogeneity factor, C_e is the concentration of adsorbate at equilibrium (mg/g), and n is the adsorption intensity between CPT and CNF.

The Temkin adsorption model reflects indirect interaction between adsorbate-adsorbate throughout the adsorption process and depicts the monolayer coverage. Taking into account the concentrations of intermediate ion, the model concludes that adsorbate binds and covers the adsorbent's surface; the heat of adsorption would fall linearly instead of logarithmically (Temkin 1940). When the experimental data best fit the Temkin isotherm, the following parameters were predicted, such as B (Temkin isotherm constant related to the heat of sorption). The positive value of B value would demonstrate that CPT binds to CNF in an exothermic process, whereas a

negative value would demonstrate an endothermic process. The linearized equation is expressed as Eq. 6.

$$Q_e = \frac{RT}{B_t} \ln(A_t) + \frac{RT}{B_t} \ln(C_e) \quad (6)$$

$$B = \frac{RT}{B_t} \quad (7)$$

where T is the absolute temperature in kelvin (298 K), R is the universal gas constant (8.314 J/(mol k)), A_t is the equilibrium binding constant, B is the constant related to heat of sorption (J/mol), and B_t is the Temkin isotherm constant related to the heat of sorption.

The Dubinin-Radushkevich (D-R) is usually applied to emphasize the process of adsorption taking place on both homogeneous as well as heterogeneous surfaces. It provides information related to interactions between the adsorbate and adsorbent, energy distribution, and type of adsorption (Sarici-Özdemir and Önal 2018). The prediction of the physical adsorption process best fits a multilayer coverage exhibiting Van der Waals interactions, whereas the chemical adsorption prediction best fits monolayer coverage, demonstrating the covalent bond arrangement (Itodo and Itodo 2010). The linear form of D-R is expressed as Eq. 8.

$$\ln Q_e = \ln Q_m - \beta \varepsilon^2 \quad (8)$$

$$\varepsilon = RT \ln \left[1 + \frac{1}{C_e} \right] \quad (9)$$

where Q_e is the amount of drug adsorbed per unit weight of sorbent (mg/g), Q_m is the maximum adsorption capacity (mg/g), β is the D-R sorption mean energy constant (mol^2/kJ^2), ε is the D-R constant, T (Kelvin) is the temperature, and $R = 0.008314$ is the gas constant (kJ/mol K).

It was found that when mean free energy value is below 8 kJ/mol, physical adsorption takes place, and when the mean free energy value is more than 8 kJ/mol, then the chemical adsorption occurs (Javadian et al. 2013). The energy value (E) is estimated by using Eq. 10.

$$E = 1/\sqrt{2\beta} \quad (10)$$

In vitro release studies at different physiological condition

The in vitro drug release profile of drug from CNF was evaluated under sink environment at different simulated physiological conditions. Briefly, freeze-dried CPT-loaded nanofibers were re-dispersed in 10 ml of simulated media of different pH, with constant shaking and incubated at 37 °C, respectively. The pH 1.2 was prepared to mimic the gastric fluid, pH 6.8 to mimic the intestinal fluid, and pH 7.4 corresponds to the

physiological conditions (phosphate buffer saline (PBS) solution). The buffer solution of pH 1.2 was prepared using NaCl, HCl, and deionized water, whereas the buffer solution of pH 6.8 was prepared using K₂HPO₄, NaOH, and deionized water. The release of CPT was determined by taking aliquots of 1 ml of the sample at specified time intervals, and the medium was replaced to retain the sink environment. The drug-loaded particles were separated from the media using centrifugation. The amount of CPT released was quantified using UV-visible spectrophotometer by evaluating the absorbance after precise time intervals at 367 nm. The drug release (%) was estimated with respect to the total amount of drug entrapped into the nanofibers (Eq. 11).

$$\begin{aligned} \text{Drug release (\%)} & \quad (11) \\ &= \frac{\text{Released drug}}{\text{The total amount of drug entrapped in nanofibers}} \times 100 \end{aligned}$$

Mathematical modeling and release kinetics

To understand the mechanism of CPT release from CNF, the CPT release data was evaluated by five release kinetics models (Costa and Sousa Lobo 2001)

- (i) Zero-order release kinetics ($W = Kt$), where W is the percentage of drug released at time “ t ” and K is the release rate constant,
- (ii) First-order kinetics ($\log W = \log W_0 - Kt/2.303$), where W_0 is the initial concentration of the drug, K is the first-order constant, and t is the release time,
- (iii) Higuchi kinetics ($Wt = K_H t^{1/2}$), where K_H is the Higuchi release rate constant,
- (iv) Korsmeyer-Peppas kinetics model ($Wt/We = Kt^n$), where Wt/We are the fractional drug release, and K is the constant, and n is the release exponent, which provides evidence about the mechanism of the drug release.
- (v) Hixson-Crowell kinetics model ($W_0^{1/3} - Wt^{1/3} = Kt$), where Wt is the amount of drug released in time “ t ,” W_0 is the initial amount of drug, and K is the constant.

Results and discussion

Morphology, particle size, and polydispersity index of prepared formulations

The understanding of the mechanism of the drug binding can be analyzed through morphological studies as any dimensional change may provide useful information. Scanning electron microscopy (SEM) of the CNF before and after loading of CPT is shown in Fig. 2. SEM images show the CNF

interconnected network-like structure and porous matrix (Fig. 2a). After drug loading, the drug crystals were found adsorbed onto the CNF surface with a matrix-type layered structure (Fig. 2 b, c, and d), which may be due to the physical adsorption of the drug. Previous reports also show similar data (Bhandari et al. 2017). The particle size distribution of the enzyme-hydrolyzed CNF is 105.7 nm published previously (Kumari et al. 2019). However, the increase in particle size was observed after the loading of CPT (Table 1). The particle size distribution was estimated by a dynamic light scattering (DLS) technique. While dealing with polydisperse nanoparticles, DLS is unable to differentiate between nanoparticles with the difference in the diameter as the scattered light of larger particles or aggregates overlays the smaller particles. The DLS generally measures the hydrodynamic diameter of the particles, including hydration shell, polymer shells, or stabilizer, which leads to increment in the particle size (Fissan et al. 2014). After CPT loading, the increment in particle size may be due to the aggregation of the drug molecule onto the CNF. The term polydispersity index (PDI) is used to describe the percentage of size distribution within the sample. The PDI generally ranges from 0.0 (uniform sample) to 1.0 (highly polydisperse samples with numerous particle size distribution). The value of 0.2 and less than 0.2 are acceptable for the polymer-based nanoparticles (Clarke 2013). The PDI value of 0.2 in 10:3 composition ratio of CNF:CPT is acceptable for drug delivery applications (Table 1). It was reported that PDI value of 0.3 and below is found to be suitable and indicates a homogeneous population of lipid-based carriers (Chen et al. 2011; Putri et al. 2017)

Encapsulation efficiency, drug loading, and isotherm studies of the prepared formulations

A prerequisite for healthcare formulations using the polymeric carrier system is high entrapment efficiency and drug loading capacity (Aditya et al. 2013). To check the suitability of the nanocarrier as a drug carrier, its ability to encapsulate and slow the release of the active therapeutics was quantitatively established. The encapsulation efficiency (EE) and loading capacity (LC) were calculated based on the solid-phase analysis at different time points (Fig. 3b). The EE and LC were evaluated at different time points to determine the time taken for the maximum incorporation of the drug into the CNF matrix. It was found that the highest EE, i.e., 65.28%, was observed in the 10:3 composition ratio of CNF-CPT, in comparison with 10:5 and 10:7. The quantification of the CPT was done using a calibration curve (Fig. 3a). The EE was decreased with an increase in the amount of CPT. The EE corresponds to the percentage of CPT incorporated into the CNF, from a given amount of CPT used, which is comparatively higher in the CNF-CPT (10:3) ratios. This suggests that as the CPT increases in CNF-CPT ratios, incorporation of the

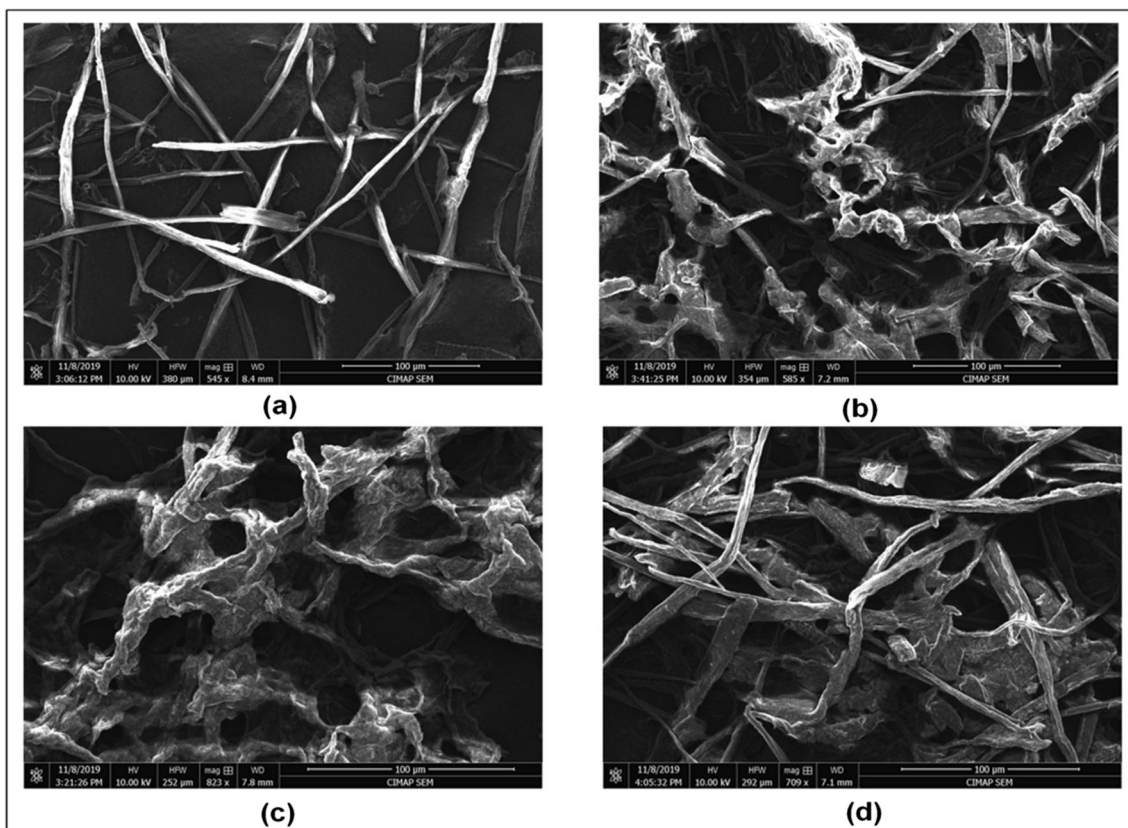


Fig. 2 SEM micrograph of **a** cellulose nanofibers alone and drug-loaded cellulose nanofibers at different composition ratio. **b** 10:3 CNF-CPT. **c** 10:5 CNF-CPT. **d** 10:7 CNF-CPT

CPT from the solvent into the CNF matrix is limited by the solubility of the drug in water and independent of the quantity of the CNF present (Tam et al. 2016). In the case of a 10:3 ratio of CNF-CPT, the low amount of drug was well solvated and easily incorporated into the matrix of CNF after 3 h (Kumari et al. 2010; Chi et al. 2019). However, as the CPT content increases in other CNF-CPT ratios, the drug content limits its solubility and proper incorporation in the CNF. Due to the presence of high CPT content, the time taken by the 10:5 and 10:7 CNF-CPT ratio is only 30 min. Similar results have been observed previously, which displayed the EE in CNF generally governed by the drug solubility in the solvent and antisolvent and not on the polymer to drug ratios (Chow et al. 2015; Tam et al. 2016).

The drug loading capacity corresponds to the amount of CPT-loaded per unit weight of the CNF. Results show that the drug loading increases with the amount of drug increase

in the CNF-CPT ratios, i.e., 10:3, 10:5, and 10:7 (Table 1), with the constant amount of CNF being used for encapsulating the different amount of drug. Presumably, it is because the interconnected CNF matrix structures were favorable to load hydrophilic CPT and the occurrence of intermolecular interaction via hydrogen bonding (Mishra et al. 2016). So, with the increase in CPT content in the CNF-CPT ratio, the loading capacity of the CNF increases. Few previous reports demonstrate lower loading capacity in the range of 1–5% (Chen et al. 2012), which is much lower compare with enzyme-mediated CNF shown in the present study (Table 1). These results confirm high encapsulation efficiency with a better loading capacity in the 10:3 CNF-CPT ratio. Therefore, this formulation has been chosen for controlled release characteristics.

To demonstrate the mechanism of adsorption of the CPT with the CNF, different isotherms were applied, such as Langmuir, Freundlich, Dubinin-Radushkevich, and Temkin

Table 1 Encapsulation efficiency, drug loading, particle size, and polydispersity index of the prepared formulations

CNF:CPT formulations	Encapsulation efficiency (%)	Drug loading capacity (%)	Particle size (DLS) (nm)	Polydispersity index
10:3	65.28 ± 3.47	19.58 ± 0.86	458.7	0.20
10:5	54.58 ± 1.02	27.29 ± 0.51	531.2	0.26
10:7	59.14 ± 4.40	41.40 ± 3.08	825.0	0.23

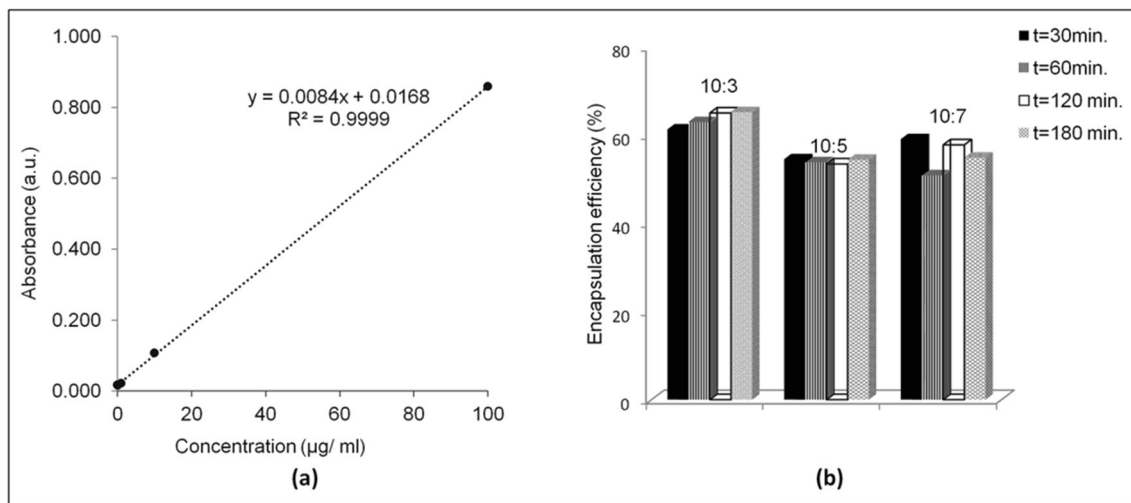


Fig. 3 **a** Graphical view of calibration curve of camptothecin and **b** encapsulation efficiency (%) of the drug-loaded fibers at different CNF-CPT ratios at different time intervals

as the CNF make the network-like structure and consist of the porous matrix. The calculated parameters like isotherm constants (b, K_f, ε) and other parameters are shown in Table 2. The correlation coefficient value (R^2) was used to find which model best depicts the adsorption mechanism. Considering the R^2 value, the adsorption of the CPT onto the CNF fits well with all the four isotherms, i.e., D-R (0.99), Temkin (0.99), Langmuir (0.94), and Freundlich isotherm (0.92) (Table 2). The good fit of the D-R isotherm model is evident that the adsorption occurred on homogeneous as well as heterogeneous surfaces (Pandian et al. 2017). The data demonstrate that the adsorption follows a pore-filling mechanism (Vijayaraghavan et al. 2006). It assumes multilayer characteristics which involve Van der Waals force, relevant for physical adsorption processes (Ayawei et al. 2017). The mean free energy less than 8 kJ/mol, i.e., 0.0016, demonstrates the involvement of physical adsorption in the uptake of CPT onto the CNF, also seen in the SEM analysis (Fig. 2b–d; Table 2).

The Temkin isotherm constant B displayed the maximal binding energy or the heat of adsorption that takes place with the coverage of the adsorbent. Based on the Temkin isotherm data, the positive value of constant B is 240.37 J/mol, which indicates the exothermic adsorption process, representing the physical adsorption. Langmuir isotherm demonstrates monolayer and homogeneous adsorption process with all binding sites possessing an equal affinity for adsorbate, i.e., CPT. The separation factor (R_L) for CPT used in this study (R_L) ranges between $0 > R_L > 1$ (Table 2), indicating linear adsorption (Dada et al. 2012). The difference adsorption capacity (Table 2) may be due to the difference in adsorption properties (Bée et al. 2011; Dubey et al. 2016).

The coefficient correlation obtained for Freundlich isotherm suggests that CPT also binds in multilayer, indicating the non-restrictive and exponential form of binding. In multilayer adsorption, the CPT molecules are not necessarily

similar to the particular number of binding sites on to the CNF surface due to exponential adsorption of CPT molecules, which occurs because of the interaction with other CPT molecules (Liu 2015). Based on the Freundlich isotherm, the $1/n$ specifies the binding strength between the CNF and CPT. The exponent value showed $1/n > 1$ (1.11) depicting the cooperative adsorption (Table 2). The cooperative adsorption usually favored by multilayer coverage of CPT into the CNF. Furthermore, the n value should be in the range of 1 to 10, which is observed from the Freundlich isotherm (Table 2) (approx.1.0), indicating the favorable adsorption between the CPT and CNF (Dada et al. 2012). From SEM images, it was confirmed that the CNF are interconnected network-like

Table 2 Langmuir, Freundlich, Dubinin-Radushkevich, and Temkin isotherm parameters for loading of CPT on CNF

Isotherms	Constants	Values
Langmuir	Qo (mg/g)	833.33
	b	0.0006
	R_L	1.00
	R^2	0.94
Freundlich	$1/n$	1.11
	n	0.90
	K_f	2.59
	R^2	0.92
Dubinin-Radushkevich	Qm (mg/g)	13.22
	ε (mol ² /kJ ²)	0.0023
	E (kJ/mol)	0.0016
	R^2	0.99
Temkin	A_t	103.7099
	B_t	10.30733
	B	240.37
	R^2	0.9984

structure and porous matrix, which may be forming monolayer as well as multilayer surfaces. Therefore, the good fit of all the isotherms indicates adsorption of CPT on to the CNF matrix according to the availability of overlapping surface matrix. Therefore, both the monolayer and multilayer type of coverage is expected. Similarly, as it is a network-like matrix with possible irregular thickness, therefore, homogeneous and heterogeneous mode of drug binding mechanism is also probable.

Interaction studies of the CPT and CNF

The interaction between the CNF and the drug was also assessed by FT-IR spectroscopy. The FT-IR spectra of CNF, CPT, and CNF-CPT are shown in Fig. 4. Each sample showed strong bands around 3400 cm^{-1} , which were attributed to O–H vibrations and depicted the broad intra and intermolecular hydrogen bonding and hydrophilic behavior of the CNF (Chirayil et al. 2014). It was described that rod-like fibers appeared aggregated due to hydrogen bonding and Van der Waals attractions. The symmetrical and asymmetrical stretching of CH vibrations were observed at 2924 cm^{-1} in CNF and CNF-CPT (Alemdar and Sain 2008). In the case of CNF-CPT, the two adsorption bands at 2919 and 2850 cm^{-1} were attributed to CH_2 and CH vibrations in CNF and benzene ring of CPT, which confirms the chemical interaction between CPT and CNF (Acevedo-Morantes et al. 2013). The carboxylic group and stretching vibrations of ester and lactone carbonyl groups were observed around 1744 cm^{-1} in CPT and CNF-CPT, which was not present in the spectra of CNF. The adsorption band between 1600 and 1700 demonstrate the

aromatic combination, present in the CPT and CNF-CPT complex (Acevedo-Morantes et al. 2013). The peak around 1600 cm^{-1} is associated with water molecules adsorbed into the cellulose fiber structure in CNF and CNF-CPT samples (Li et al. 2016). It has been reported that the adsorption band between 1600 and 1650 cm^{-1} demonstrates the stretching vibration of the benzene ring, shown in CPT and CNF-CPT (Zhao et al. 2010). The absorption peak of stretching and bending vibrations were observed at 1431 , 1369 , 1325 , 1054 , and 899 cm^{-1} , which were attributed to $-\text{CH}_2$, $-\text{CH}$, $-\text{OH}$, and $\text{C}-\text{O}$ bonds in CNF (Xu et al. 2013). The shifting of peaks in CNF-CPT before and after drug binding showed the intermolecular interaction through hydrogen bonding (Mishra et al. 2016). Hence, the FT-IR results confirm the chemical interaction between the CPT and CNF.

In vitro release of CPT and release kinetics at different pH conditions

Drug release is a complex process during which drug mass transport through diffusion is an important mechanism (Siepmann and Siepmann 2012). The CNF exhibited a slow release of CPT (up to 4.4%) from time 0 to 6 h, followed by which 14.38% release of CPT took place from 6 to 48 h at pH 1.2 condition. Drug release at pH 6.8 also showed a slow release pattern for CPT, i.e., 26.2% release takes place from 0 to 6 h, followed by 63.4% release of CPT from 6 to 48 h. In the case of pH 7.4, the CPT release was observed as 24.8% up to 6 h, and 80.2% CPT release took place from 6 to 48 h (Fig. 5). The results confirmed a slow and extended-release pattern of CPT from the CNF at different simulated pH conditions with

Fig. 4 FT-IR spectra of the cellulose nanofibers (CNF), camptothecin (CPT), and camptothecin loaded nanofibers (CNF-CPT)

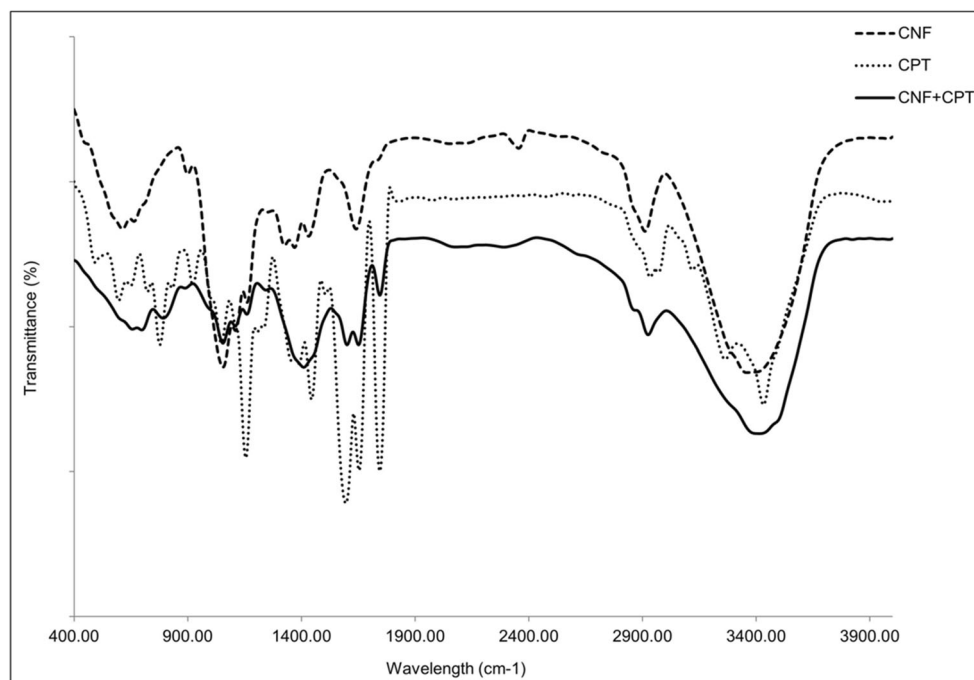
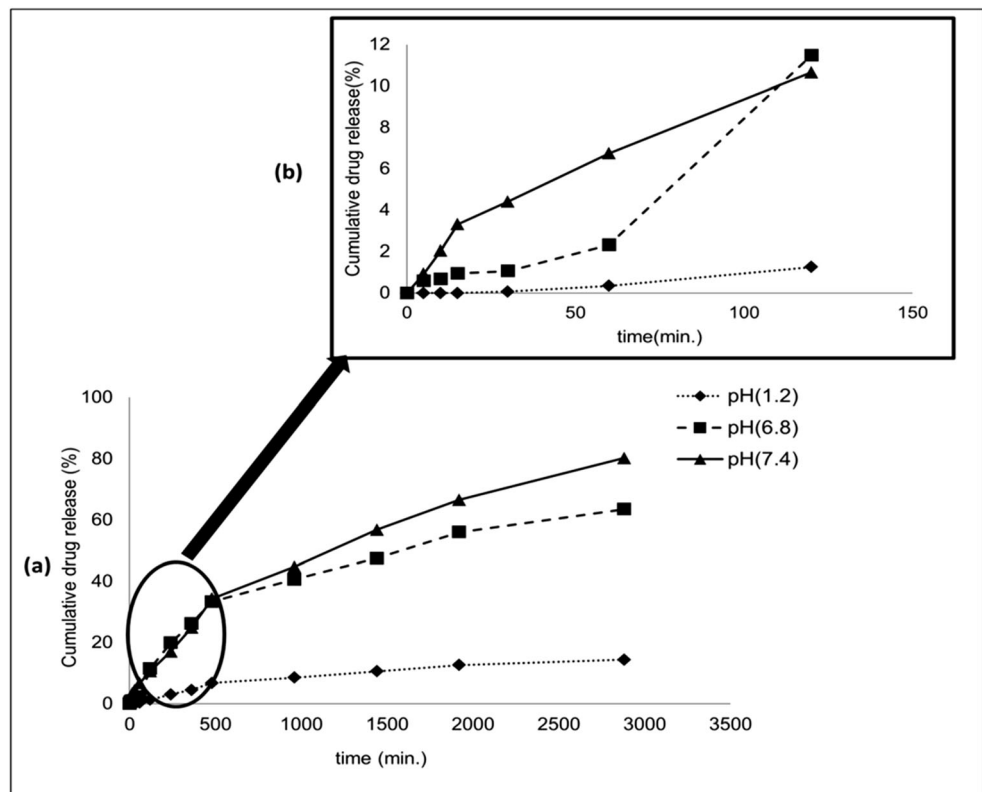


Fig. 5 Drug release graph showing a cumulative release of camptothecin at different pH conditions



no initial burst effect. A slow and extended-release of CPT could be due to the matrix structure and swelling behavior of the carrier system with regard to pH, which is allowing the controlled and stable transport of drugs. The hydrophobic behavior plays a significant role in drug release; the interaction between hydrophobic drugs and hydrophobic core is often responsible for the slow release pattern of the drug from the nanoparticles (Sutton et al. 2007; Tran et al. 2014). The controlled and extended-release pattern without any burst release also demonstrates that CPT was fully adsorbed into the CNF matrices, which is also supported by isotherm studies. The most significant limitations in the drug delivery process are the complications of complete encapsulation and retention, followed by prolonged release and targeted delivery of therapeutics. For complex diseases like cancer, the extended-release nanocarriers are considered as attractive therapeutic agents due to their prolonged drug release behavior (Prosperi et al. 2017). Therefore, in addition to CPT, most likely, these CNF could be beneficial for the delivery of other anticancer drugs.

The drug release mechanism of CPT from CNF at different pH levels was evaluated by employing several mathematical models such as zero order, first order, Higuchi, Korsmeyer-Peppas, and Hixson-Crowell (Costa and Sousa Lobo 2001). Table 3 demonstrates the coefficient correlation values (R^2) obtained after the model fitting of release data at different pH. The graphical representation of the fitted models has been

shown in Fig. 6. The results showed that release data were best fitted to Higuchi model at pH 1.2 (R^2 value 0.98), at pH 6.8 (R^2 value 0.97), and at pH 7.4 (R^2 value 0.99). The best fitted Higuchi model showed that the release of the drug was governed by the diffusion mechanism at all pH conditions. Moreover, the release data was also good fitted to Korsmeyer-Peppas models at pH 1.2 (R^2 value 0.94) and 7.4 (R^2 value 0.98) and slightly fitted at pH 6.8 (R^2 value 0.90).

In Korsmeyer-Peppas model, n is the diffusional exponent, which is the characteristic parameter of the transport mechanism. The n value of 0.45 is correlated to Fickian diffusion mechanism and drug release governed by diffusion, $0.45 < n < 0.89$ correlated to non-Fickian or anomalous transport and governed by diffusion and swelling, $1.0 < n$ corresponds to non-Fickian (case II) or zero-order release kinetics, and release of drug governed by swelling or relaxation of polymeric chain (Costa and Sousa Lobo 2003; Mhlanga and Ray 2015). From the results, exponent (n) is 0.23 at pH 1.2, 0.51 at pH 6.8, and 0.91 at pH 7.4 demonstrating that release of drug was controlled by non-Fickian diffusion mechanism at pH 1.2, 6.8, and case II transport mechanism, indicating that the drug release was followed by diffusion, swelling, and polymer relaxation due to erosion of the polymer (Gao et al. 2013). The Korsmeyer-Peppas model helps to understand the contribution of diffusion and polymer relaxation in the drug release pattern. The release data were found not best fitted to the zero-

Table 3 Mathematical models and correlation values (R^2) based on release data

Kinetics models	Correlation equation	pH (1.2)	pH (6.8)	pH (7.4)
First order	$y =$	$0.0004x + 0.2457$	$0.0006x + 0.5033$	$0.0006x + 0.6921$
	R^2	0.70	0.54	0.61
Zero order	$y =$	$0.0053x + 1.5517$	$0.0239x + 7.1767$	$0.0303x + 7.1583$
	R^2	0.89	0.85	0.93
Korsmeyer-Peppas	$y =$	$0.605x - 0.9148$	$0.6865x - 0.5129$	$0.626x - 0.2357$
	R^2	0.93	0.89	0.97
Higuchi	$y =$	$0.3141x - 1.5008$	$1.3178x - 2.3994$	$1.6132x - 3.9131$
	R^2	0.98	0.97	0.99
Hixson-Crowell	$y =$	$9E-05x + 0.0244$	$0.0005x + 0.1097$	$0.0007x + 0.0846$
	R^2	0.89	0.91	0.98

order and Hixson-Crowell models at any of the pH conditions and did not show a higher correlation coefficient at pH 1.2 and 6.8. The data was not fitted to the first-order equation, so the graphical representation was not shown in the manuscript.

Conclusion

The present study showed an application of a green synthesized biodegradable CNF as a promising nanocarrier system. A CNF-CPT composite has been prepared. The morphological and isotherm studies showed the physical absorption of

CPT into the CNF matrices. The CNF-CPT formulation of a 10:3 ratio displayed a controlled and extended-release of CPT at three different physiological pH conditions, which is generally an essential requirement in the pharmaceutical applications. The controlled and extended drug release profile is governed by diffusion, swelling, polymer relaxation/erosion, and drug carrier interaction mechanisms as predicted by the release kinetics studies. Henceforth, it is concluded that the green synthesized CNF could be a promising nanocarrier for the problematic drugs. However, in the future, cell-based and animal studies are needed to demonstrate the complete efficacy of the nanocarriers.

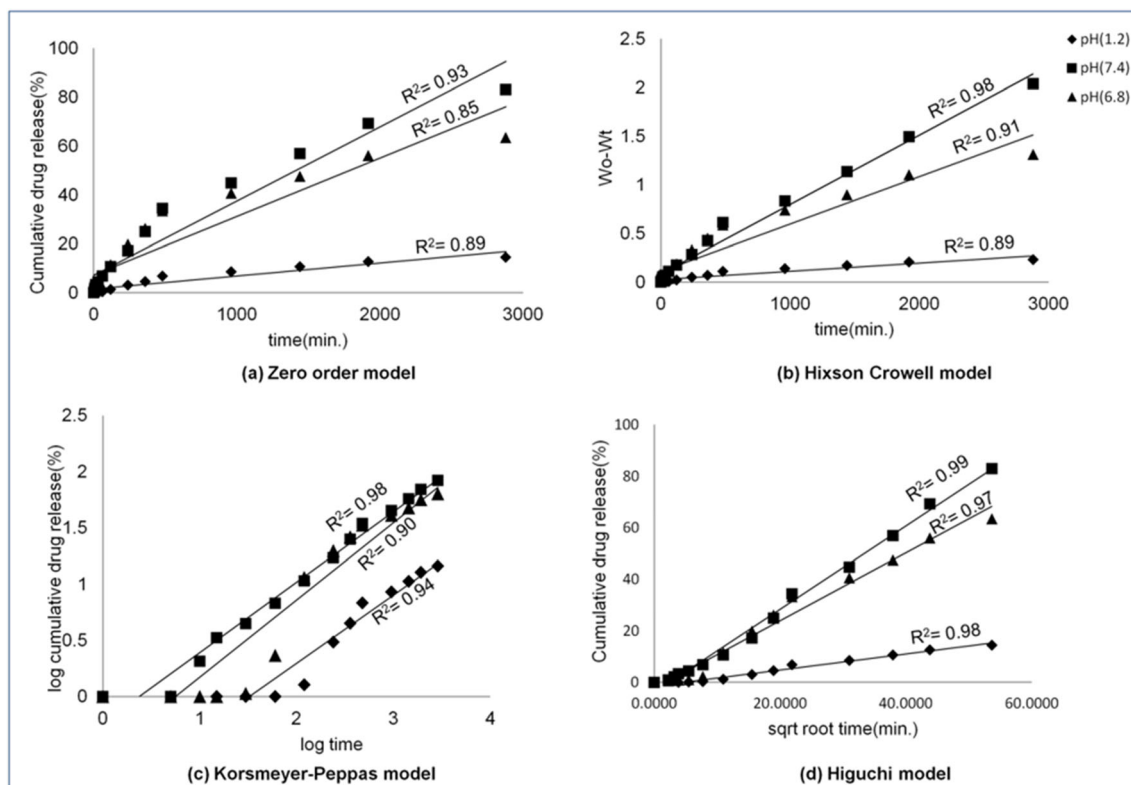


Fig. 6 Drug release kinetics plots. **a** Zero order. **b** Hixson-Crowell. **c** Korsmeyer-Peppas. **d** Higuchi models

Acknowledgments The authors are thankful to the Director, CSIR-CIMAP, Lucknow, for the necessary facilities required to complete the experimental work. The authors acknowledge Dr. P.V. Ajayakumar, Chief Scientist, and Dr. Pooja Singh, Technical Assistant CSIR-CIMAP for SEM analysis and Dr. Apama Chaudhary for the drug release data analysis support. The authors also acknowledge Prof. B.C. Yadav (In-charge), USIC facility, Babasaheb Bhimrao Ambedkar University, for FT-IR analysis.

Funding information This work was financially supported by CSIR-Aroma Mission Project (HCP 007). PK acknowledges University Grants Commission, New Delhi, for financial assistance.

Compliance with ethical standards

Conflict of interest The authors declare that they have no conflicts of interest.

References

Abe K, Iwamoto S, Yano H (2007) Obtaining cellulose nanofibers with a uniform width of 15 nm from wood. *Biomacromolecules* 8:3276–3278. <https://doi.org/10.1021/BM700624P>

Acevedo-Morantes CY, Acevedo-Morantes MT, Suleiman-Rosado D, Ramirez-Vick JE (2013) Evaluation of the cytotoxic effect of camptothecin solid lipid nanoparticles on MCF7 cells. *Drug Deliv* 20:338–348. <https://doi.org/10.3109/10717544.2013.834412>

Aditya NP, Shim M, Lee I, Lee Y, Im MH, Ko S (2013) Curcumin and genistein coloaded nanostructured lipid carriers: in vitro digestion and antiprostata cancer activity. *J Agric Food Chem* 61:1878–1883. <https://doi.org/10.1021/jf305143k>

Alemdar A, Sain M (2008) Isolation and characterization of nanofibers from agricultural residues – wheat straw and soy hulls. *Bioresour Technol* 99:1664–1671. <https://doi.org/10.1016/J.BIORTECH.2007.04.029>

Ali A, Ahmed S (2018) A review on chitosan and its nanocomposites in drug delivery. *Int J Biol Macromol* 109:273–286. <https://doi.org/10.1016/J.IJBIOMAC.2017.12.078>

Ayawei N, Ebelegi AN, Wankasi D (2017) Modelling and interpretation of adsorption isotherms. *J Chem* 2017:1–11. <https://doi.org/10.1155/2017/3039817>

Bardet R, Bras J (2014) Cellulose nanofibers and their use in paper industry. In: *Handbook of Green materials: 1 Bionanomaterials: separation processes, characterization and properties*, pp 207–232

Bée A, Talbot D, Abramson S, Dupuis V (2011) Magnetic alginate beads for Pb(II) ions removal from wastewater. *J Colloid Interface Sci* 362:486–492. <https://doi.org/10.1016/J.JCIS.2011.06.036>

Bhandari J, Mishra H, Mishra PK, Wimmer R, Ahmad FJ, Talegaonkar S (2017) Cellulose nanofiber aerogel as a promising biomaterial for customized oral drug delivery. *Int J Nanomedicine* 12:2021–2031. <https://doi.org/10.2147/IJN.S124318>

Chen KJ, Tang L, Garcia MA, Wang H, Lu H, Lin WY, Hou S, Yin Q, Shen CK, Cheng J, Tseng HR (2012) The therapeutic efficacy of camptothecin-encapsulated supramolecular nanoparticles. *Biomaterials* 33:1162–1169. <https://doi.org/10.1016/J.BIOMATERIALS.2011.10.044>

Chen M, Liu X, Fahr A (2011) Skin penetration and deposition of carboxyfluorescein and temoporfin from different lipid vesicular systems: in vitro study with finite and infinite dosage application. *Int J Pharm* 408:223–234. <https://doi.org/10.1016/j.ijpharm.2011.02.006>

Cherian BM, Pothan LA, Nguyen-Chung T, Mennig G, Kottaisamy M, Thomas S (2008) A novel method for the synthesis of cellulose

nanofibril whiskers from banana fibers and characterization. *J Agric Food Chem* 56:5617–5627. <https://doi.org/10.1021/jf8003674>

Chi Y, Wang Z, Wang J, Dong W, Xin P, Bi J, Jiang T, Chen CP (2019) Dimeric camptothecin-loaded mPEG-PCL nanoparticles with high drug loading and reduction-responsive drug release. *Colloid and Polymer Science* 1–8. doi: <https://doi.org/10.1007/s00396-019-04581-8>

Chirayil CJ, Joy J, Mathew L, Mozetic M, Koetz J, Thomas S (2014) Isolation and characterization of cellulose nanofibrils from *Helicteres isora* plant. *Ind Crop Prod* 59:27–34. <https://doi.org/10.1016/J.INDCROP.2014.04.020>

Chow SF, Wan KY, Cheng KK, Wong KW, Sun CC, Baum L, Chow AH (2015) Development of highly stabilized curcumin nanoparticles by flash nanoprecipitation and lyophilization. *Eur J Pharm Biopharm* 94:436–449. <https://doi.org/10.1016/j.ejpb.2015.06.022>

Çirpanli Y, Bilensoy E, Lale Doğan A, Çaliş S (2009) Comparative evaluation of polymeric and amphiphilic cyclodextrin nanoparticles for effective camptothecin delivery. *Eur J Pharm Biopharm* 73:82–89. <https://doi.org/10.1016/J.EJPB.2009.04.013>

Clarke SP (2013) Development of hierarchical magnetic nanocomposite materials for biomedical applications (Doctoral dissertation, Dublin City University)

Clift MJD, Gehr P, Rothen-Rutishauser B (2011) Nanotoxicology: a perspective and discussion of whether or not in vitro testing is a valid alternative. *Arch Toxicol* 85(7):723–731

Costa P, Sousa Lobo JM (2003) Evaluation of mathematical models describing drug release from estradiol transdermal systems. *Drug Dev Ind Pharm* 29:89–97. <https://doi.org/10.1081/DDC-120016687>

Costa P, Sousa Lobo JM (2001) Modeling and comparison of dissolution profiles. *Eur J Pharm Sci* 13:123–133. [https://doi.org/10.1016/S0928-0987\(01\)00095-1](https://doi.org/10.1016/S0928-0987(01)00095-1)

Costache AD, Sheihet L, Zaveri K, Knight DD, Kohn J (2009) Polymer–drug interactions in tyrosine-derived triblock copolymer nanospheres: a computational modeling approach. *Mol Pharm* 6:1620–1627. <https://doi.org/10.1021/mp900114w>

Dada AO, Olalekan AP, Olatunya AM, Dada OJ (2012) Langmuir, Freundlich, Temkin and Dubinin–Radushkevich isotherms studies of equilibrium sorption of Zn²⁺ onto phosphoric acid modified rice husk. *IOSR J Appl Chem* 3:38–45. <https://doi.org/10.9790/5736-0313845>

Deepa B, Abraham E, Cordeiro N, Mozetic M, Mathew AP, Oksman K, Faria M, Thomas S, Pothan LA (2015) Utilization of various lignocellulosic biomass for the production of nanocellulose: a comparative study. *Cellulose* 22:1075–1090. <https://doi.org/10.1007/s10570-015-0554-x>

Dubey R, Bajpai J, Bajpai AK (2016) Chitosan-alginate nanoparticles (CANPs) as potential nanosorbent for removal of Hg (II) ions. *Environ Nanotechnol Monit Manag* 6:32–44. <https://doi.org/10.1016/J.ENMM.2016.06.008>

Esmaeili A, Rafiee R (2015) Preparation and biological activity of nanocapsulated *Glycyrrhiza glabra* L. var. *glabra*. *Flavour Fragr J* 30:113–119. <https://doi.org/10.1002/ffj.3225>

Fan N, Duan K, Wang C, Liu S, Luo S, Yu J, Huang J, Li Y, Wang D (2010) Fabrication of nanomicelle with enhanced solubility and stability of camptothecin based on α,β -poly[(N-carboxybutyl)-l-aspartamide]-camptothecin conjugate. *Colloids Surf B: Biointerfaces* 75:543–549. <https://doi.org/10.1016/j.colsurfb.2009.09.034>

Filson PB, Dawson-Andoh BE, Schwegler-Berry D (2009) Enzymatic-mediated production of cellulose nanocrystals from recycled pulp. *Green Chem* 11:1808. <https://doi.org/10.1039/b915746h>

Fissan H, Ristig S, Kaminski H, Asbach C, Epple M (2014) Comparison of different characterization methods for nanoparticle dispersions before and after aerosolization. *Anal Methods* 6:7324. <https://doi.org/10.1039/C4AY01203H>

Fonseca LM, dos Santos Cruxen CE, Bruni GP, Fiorentini ÂM, da Rosa ZE, Lim LT, Dias AR (2019) Development of antimicrobial and antioxidant electrospun soluble potato starch nanofibers loaded with

- carvacrol. *Int J Biol Macromol* 139:1182–1190. <https://doi.org/10.1016/j.IJBIOMAC.2019.08.096>
- Gao Y, Li LB, Zhai G (2008) Preparation and characterization of Pluronic/TPGS mixed micelles for solubilization of camptothecin. *Colloids Surf B: Biointerfaces* 64:194–199. <https://doi.org/10.1016/j.COLSURFB.2008.01.021>
- Gao Y, Zuo J, Bou-Chacra N, Pinto TD, Clas SD, Walker RB, Löbenberg R (2013) In vitro release kinetics of antituberculosis drugs from nanoparticles assessed using a modified dissolution apparatus. *Biomed Res Int* 2013:2013. <https://doi.org/10.1155/2013/136590>
- Hu X, Liu S, Zhou G, Huang Y, Xie Z, Jing X (2014) Electrospinning of polymeric nanofibers for drug delivery applications. *J Control Release* 185:12–21. <https://doi.org/10.1016/j.jconrel.2014.04.018>
- Huang SH, Chen DH (2009) Rapid removal of heavy metal cations and anions from aqueous solutions by an amino-functionalized magnetic nano-adsorbent. *J Hazard Mater* 163:174–179. <https://doi.org/10.1016/j.jhazmat.2008.06.075>
- Itodo AU, Itodo HU (2010) Sorption energies estimation using Dubinin-Radushkevich and Temkin adsorption isotherms. *Life Sci J* 4:31–39
- Javadian H, Ahmadi M, Ghiasvand M, Kahrizi S, Katal R (2013) Removal of Cr(VI) by modified brown algae *Sargassum bevanom* from aqueous solution and industrial wastewater. *J Taiwan Inst Chem Eng* 44:977–989. <https://doi.org/10.1016/j.JTICE.2013.03.008>
- Kaur H, Dutt D, Tyagi CH (2010) Optimization of soda pulping process of ligno-cellulosic residues of lemon and sofia grasses produced after steam distillation. *BioResources* 6:103–120
- Kumari A, Yadav SK, Pakade YB, Singh B, Yadav SC (2010) Development of biodegradable nanoparticles for delivery of quercetin. *Colloids Surf B: Biointerfaces* 80:184–192. <https://doi.org/10.1016/j.colsurfb.2010.06.002>
- Kumari P, Pathak G, Gupta R, Sharma D, Meena A (2019) Cellulose nanofibers from lignocellulosic biomass of lemongrass using enzymatic hydrolysis: characterization and cytotoxicity assessment. *DARU J Pharm Sci* 27:1–11. <https://doi.org/10.1007/s40199-019-00303-1>
- Li D, Wang Q, Huang F, Wei Q (2019) Electrospun nanofibers for enzyme immobilization. *Nanofabrication and Applications, Electrospinning*, pp 765–781. <https://doi.org/10.1016/B978-0-323-51270-1.00026-1>
- Li J, Zhang S, Gao B, Yang A, Wang Z, Xia Y, Liu H (2016) Characteristics and deoxy-liquefaction of cellulose extracted from cotton stalk. *Fuel* 166:196–202. <https://doi.org/10.1016/J.FUEL.2015.10.115>
- Lin N, Dufresne A (2014) Nanocellulose in biomedicine: current status and future prospect. *Eur Polym J* 59:302–325. <https://doi.org/10.1016/J.EURPOLYMJ.2014.07.025>
- Liu S (2015) Cooperative adsorption on solid surfaces. *J Colloid Interface Sci* 450:224–238. <https://doi.org/10.1016/J.JCIS.2015.03.013>
- Löbmann K, Svagan AJ (2017) Cellulose nanofibers as excipient for the delivery of poorly soluble drugs. *Int J Pharm* 533:285–297. <https://doi.org/10.1016/J.IJPHARM.2017.09.064>
- Mehrabi F, Shamspur T, Mostafavi A, Saljooqi A, Fathirad F (2017) Synthesis of cellulose acetate nanofibers and its application in the release of some drugs. *Nanomed Res J* 2:199–207. <https://doi.org/10.22034/NMRJ.2017.03.008>
- Mhlanga N, Ray SS (2015) Kinetic models for the release of the anticancer drug doxorubicin from biodegradable polylactide/metal oxide-based hybrids. *Int J Biol Macromol* 72:1301–1307. <https://doi.org/10.1016/j.ijbiomac.2014.10.038>
- Mi Z, Burke TG (1994) Differential interactions of camptothecin lactone and carboxylate forms with human blood components. *Biochemistry* 33:10325–10336. <https://doi.org/10.1021/bi00200a013>
- Mishra D, Yadav V, Khare P, Jyotshna DMR, Meena A, Shanker K (2016) Development of crystalline cellulosic fibres for sustained release of drug. *Curr Top Med Chem* 16:2026–2035
- Natesan S, Sugumaran A, Ponnusamy C, Jeevanesan V, Girija G, Palanichamy R (2014) Development and evaluation of magnetic microemulsion: tool for targeted delivery of camptothecin to BALB/c mice-bearing breast cancer. *J Drug Target* 22:913–926. <https://doi.org/10.3109/1061186X.2014.948878>
- Nguyen HN, Hoang TM, Mai TT, Nguyen TQ, Do HD, Pham TH, Nguyen TL, Ha PT (2015) Enhanced cellular uptake and cytotoxicity of folate decorated doxorubicin loaded PLA-TPGS nanoparticles. *Adv Nat Sci Nanosci Nanotechnol* 6:025005. <https://doi.org/10.1088/2043-6262/6/2/025005>
- Pandian AM, Karthikeyan C, Rajasimman M (2017) Isotherm and kinetic studies on adsorption of malachite green using chemically synthesized silver nanoparticles. *Nanotechnol Environ Eng* 2:2–17. <https://doi.org/10.1007/s41204-016-0013-4>
- Pereira MM, Raposo NR, Brayner R, Teixeira EM, Oliveira V, Quintão CC, Camargo LS, Mattoso LH, Brandão HM (2013) Cytotoxicity and expression of genes involved in the cellular stress response and apoptosis in mammalian fibroblast exposed to cotton cellulose nanofibers. *Nanotechnology* 24:075103. <https://doi.org/10.1088/0957-4484/24/7/075103>
- Prosperi D, Colombo M, Zanoni I, Granucci F (2017) Drug nanocarriers to treat autoimmunity and chronic inflammatory diseases. *Semin Immunol* 34:61–67. <https://doi.org/10.1016/j.smim.2017.08.010>
- Putri DC, Dwiastuti R, Marchaban M, Nugroho AK (2017) Optimization of mixing temperature and sonication duration in liposome preparation. *J Pharm Sci Community* 14:79–85. <https://doi.org/10.24071/jpsc.142728>
- Rezaei A, Nasirpour A, Fathi M (2015) Application of cellulose nanofibers in food science using electrospinning and its potential risk. *Compr Rev Food Sci Food Saf* 14:269–284. <https://doi.org/10.1111/1541-4337.12128>
- Salah SM (2013) Application of nano-cellulose in textile. *J Text Sci Eng* 03:1–1. <https://doi.org/10.4172/2165-8064.1000142>
- Sarici-Özdemir Ç, Önal Y (2018) Study to observe the applicability of the adsorption isotherms used for the adsorption of medicine organics onto activated carbon. *Part Sci Technol* 36:254–261. <https://doi.org/10.1080/02726351.2016.1246497>
- Shaker MA, Yakout AA (2016) Optimization, isotherm, kinetic and thermodynamic studies of Pb(II) ions adsorption onto N-maleated chitosan-immobilized TiO₂ nanoparticles from aqueous media. *Spectrochim Acta A Mol Biomol Spectrosc* 154:145–156. <https://doi.org/10.1016/j.saa.2015.10.027>
- Siepmann J, Siepmann F (2012) Modeling of diffusion controlled drug delivery. *J Control Release* 161:351–362. <https://doi.org/10.1016/J.JCONREL.2011.10.006>
- Silva P, Bonifácio B, Ramos M, Negri K, Maria Bauab T, Chorilli M (2013) Nanotechnology-based drug delivery systems and herbal medicines: a review. *Int J Nanomedicine* 9:1. <https://doi.org/10.2147/IJN.S52634>
- Sutton D, Wang S, Nasongkla N, Gao J, Dormidontova EE (2007) Doxorubicin and β -lapachone release and interaction with micellar core materials: experiment and modeling. *Exp Biol Med* 232:1090–1099. <https://doi.org/10.3181/0702-RM-31>
- Tam YT, To KK, Chow AH (2016) Fabrication of doxorubicin nanoparticles by controlled antisolvent precipitation for enhanced intracellular delivery. *Colloids Surf B: Biointerfaces* 139:249–258. <https://doi.org/10.1016/j.colsurfb.2015.12.026>
- Temkin MI (1940) Kinetics of ammonia synthesis on promoted iron catalysts. *Acta Physicochim URSS* 12:327–356
- Tran TH, Nguyen CT, Gonzalez-Fajardo L, Hargrove D, Song D, Deshmukh P, Mahajan L, Ndaya D, Lai L, Kasi RM, Lu X (2014) Long circulating self-assembled nanoparticles from cholesterol-containing brush-like block copolymers for improved drug delivery to tumors. *Biomacromolecules* 15:4363–4375. <https://doi.org/10.1021/bm5013822>

- Valo H, Kovalainen M, Laaksonen P, Häkkinen M, Auriola S, Peltonen L, Linder M, Järvinen K, Hirvonen J, Laaksonen T (2011) Immobilization of protein-coated drug nanoparticles in nanofibrillar cellulose matrices—enhanced stability and release. *J Control Release* 156:390–397. <https://doi.org/10.1016/j.jconrel.2011.07.016>
- Vasudevan S, Lakshmi J (2012) Process conditions and kinetics for the removal of copper from water by electrocoagulation. *Environ Eng Sci* 29:563–572. <https://doi.org/10.1089/ees.2010.0429>
- Vasudevan S, Lakshmi J, Kamaraj R, Sozhan G (2013) A critical study on the removal of copper by an electrochemically assisted coagulation: equilibrium, kinetics, and thermodynamics. *Asia Pac J Chem Eng* 8: 162–171. <https://doi.org/10.1002/apj.1657>
- Vázquez I, Rodríguez-Iglesias J, Marañón E, Castrillón L, Álvarez M (2007) Removal of residual phenols from coke wastewater by adsorption. *J Hazard Mater* 147:395–400. <https://doi.org/10.1016/J.JHAZMAT.2007.01.019>
- Vijayaraghavan K, Padmesh TV, Palanivelu K, Velan M (2006) Biosorption of nickel(II) ions onto *Sargassum wightii*: application of two-parameter and three-parameter isotherm models. *J Hazard Mater* 133:304–308. <https://doi.org/10.1016/J.JHAZMAT.2005.10.016>
- Xu F, Yu J, Tesso T, Dowell F, Wang D (2013) Qualitative and quantitative analysis of lignocellulosic biomass using infrared techniques: a mini-review. *Appl Energy* 104:801–809. <https://doi.org/10.1016/J.APENERGY.2012.12.019>
- Zeng J, Xu X, Chen X, Liang Q, Bian X, Yang L, Jing X (2003) Biodegradable electrospun fibers for drug delivery. *J Control Release* 92:227–231. [https://doi.org/10.1016/S0168-3659\(03\)00372-9](https://doi.org/10.1016/S0168-3659(03)00372-9)
- Zhao X, Zu Y, Li Q, Wang M, Zu B, Zhang X, Jiang R, Zu C (2010) Preparation and characterization of camptothecin powder micronized by a supercritical antisolvent (SAS) process. *J Supercrit Fluids* 51:412–419. <https://doi.org/10.1016/j.supflu.2009.10.004>

Publisher's note Springer Nature remains neutral with regard to jurisdictional claims in published maps and institutional affiliations.